Available at: http://publications.ictp.it IC/2008/099

United Nations Educational, Scientific and Cultural Organization
and
International Atomic Energy Agency

THE ABDUS SALAM INTERNATIONAL CENTRE FOR THEORETICAL PHYSICS

AN AUDIO-MAGNETOTELLURIC INVESTIGATION OF THE EASTERN MARGIN OF THE MAMFE BASIN, CAMEROON

C.T. Tabod[1]
Department of Physics, Faculty of Science, University of Yaounde I,
P.O. Box 812, Yaounde, Cameroon
and
The Abdus Salam International Centre for Theoretical Physics, Trieste, Italy,

A.-P. Tokam Kamga, E. Manguelle-Dicoum, R. Nouayou and S. Nguiya
Department of Physics, Faculty of Science, University of Yaounde I,
P.O. Box 812, Yaounde, Cameroon.

Abstract

Audio-magnetotelluric (AMT) data has been used to study the eastern margin of the Mamfe sedimentary basin along two profiles. Both profiles run across the sedimentary-metamorphic transition zone in this part of the basin. A 1-D interpretation of these data has been carried out using frequency profiling, pseudosections and geoelectric sections. Studying the propagation of the electric field at each station also gives an initial qualitative understanding of the possible layering of the subsurface at the station.

A dioritic basement intrusion into the sediments has been identified along one of these profiles and a granitic intrusion under the other. Faults have been identified along both profiles marking the transition from sedimentary to metamorphic rocks at the eastern edge of the basin. However, this transition is complex and not smooth. This also represents the eastern margin of the more extensive Benue Trough of Nigeria in its south eastern part.

MIRAMARE – TRIESTE

December 2008

[1] Corresponding author. charlestabod@yahoo.co.uk

1. Introduction

The Mamfe basin is located between latitudes 5°N and 6°N, and longitudes 8°45'E and 10°E with a maximum altitude of 300 m. One major river, the Manyu, flows right across the basin from east to west and continues into Nigeria where it is referred to as the Cross River. The Mamfe basin, like the Yola and Niger basins, is an extension of the Benue Trough, Nigeria. It is found almost midway along the Cameroon Volcanic Line (CVL), a line of volcanic centres stretching from Pagalu in the Atlantic Ocean through Mt. Cameroon to the Ngoundere and Biu Plateaux in Cameroon and Nigeria, respectively (figure 1). The Mamfe basin is believed to have resulted from basement rifting associated with the reactivation of an east-west trending mylonite zone along the Mone Faults (Dumort 1968). Like other West and Central African rift systems, the formation of the Mamfe basin is thought to be directly linked to the opening of the South Atlantic Ocean during the Middle to late Jurassic (Fairhead and Green 1989).

A geological survey of the region was undertaken by Dumort (1968) and photo-geological studies have been done by Paterson et al (1976). The Mamfe basin is made up of cretaceous series with a Precambrian basement composed of granite, migmatite and gneiss (figure 2). The cretaceous series is overlain by tertiary volcanics (basalts) in some parts of the basin. These basalts are dioritic in composition. Many intrusions of diorite and the presence of syenitic massifs are observed in the eastern part of the basin. However, the eastern margin of the basin is not yet geologically well defined.

Geophysical studies carried out in the region include gravity work by Collignon (1968), Fairhead and Okereke (1987), Fairhead and Okereke (1988), Fairhead et al (1991), Ndougsa (2004), Ndougsa Mbarga et al (2004) and Nouayou (2005). In this study, transition from sedimentary to metamorphic rocks across the eastern margin of the Mamfe basin has been examined along two audio-magnetotelluric (AMT) profiles comprising 9 stations. The study was carried out by the Department of Physics, University of Yaounde I, Cameroon, as part of a work to determine the characteristics of this basin funded by the National Hydrocarbon Cooperation (SNH).

The propagation of the electric field has been analysed to give a qualitative stratification of the subsurface beneath each station. Meanwhile, the apparent resistivity values at each station have been interpreted in one dimension through frequency profiling, pseudosections and geoelectric sections. The magnetotelluric method has been used by other workers in other regions to differentiate between formations of highly contrasting resistivities, for example, Monteiro Santos et al (2006), Nurhasan et al (2006), Ogawa et al (2002), Lilley et al (2001) and Fuji-ta et al (1997).

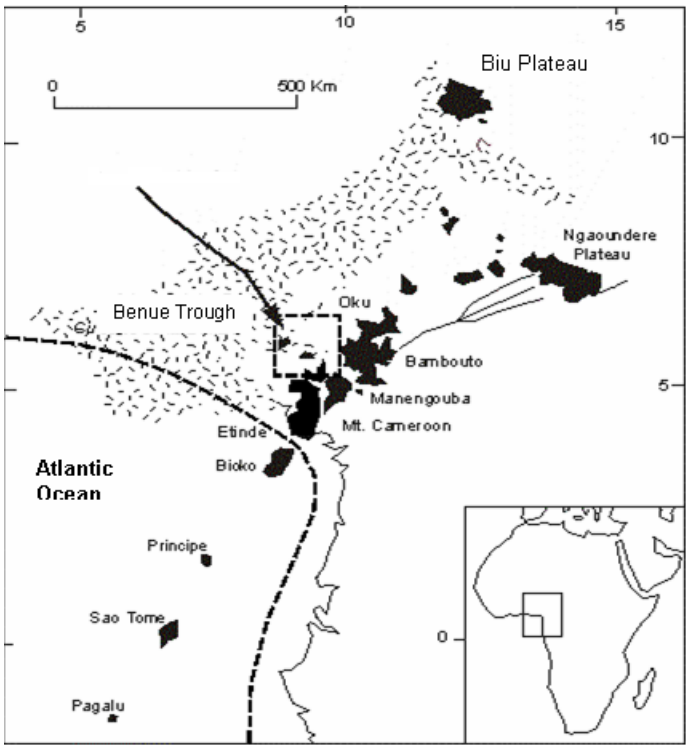

Figure **1**. Location of the Mamfe sedimentary basin. The shaded area represents sediments and the volcanics are shown as black spots (after Ngando et al 2004).

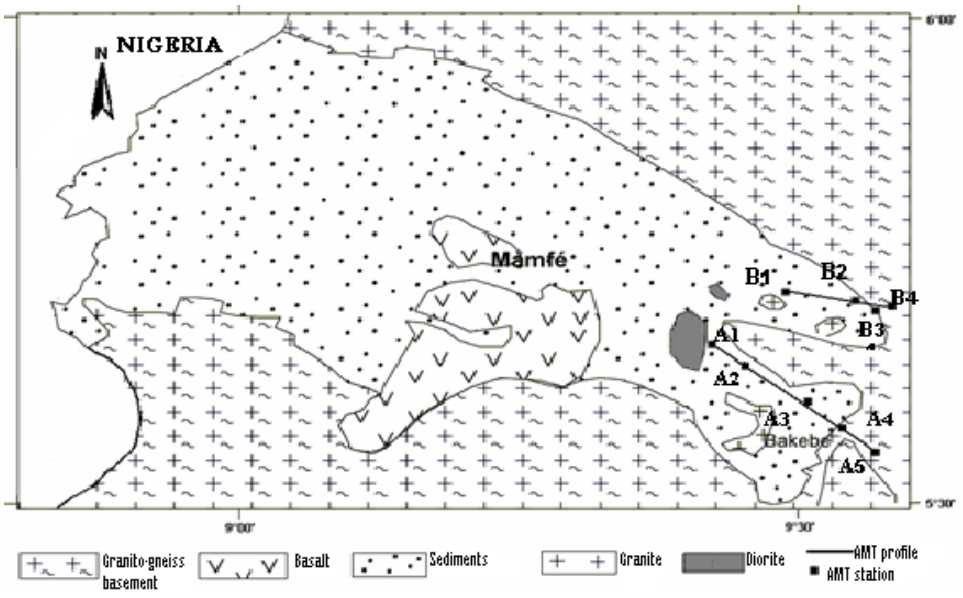

Figure **2**. Simplified geologic map of the Mamfe basin showing AMT stations (modified from Dumort 1968).

2. Method

The magnetotelluric (MT) method due to Cagniard (1953), is based on the simultaneous measurements, at the Earth's surface, of components of natural electromagnetic field induced in the earth by electromagnetic waves (assumed plane) reaching the Earth from the upper atmosphere. These

measurements are used to deduce the resistivity and depth of subsurface structures using the fundamental Cagniard relation:

$$\rho_a = 0.2\, T\, (E_x / H_y)^2$$

where E_x (mV/km) is the electric field in the *x*-direction, H_y (gammas) is the magnetic field in the *y*-direction at the same period T (s) and ρ_a (Ohm-m) is the apparent resistivity of an n-layered earth which would be the true resistivity for a homogeneous earth. The depth of penetration *P* (km) of the natural electromagnetic wave is given by:

$$P = 2\pi \sqrt{10\rho_a\, T} \;=\; 0.503\sqrt{\rho_a T}$$

The fundamental Cagniard relation is a scalar one, good for the study of one-dimensional geologic structures. For two dimensional geologic structures, the relation between the electric field **E** and the magnetic field **H** is a tensor (Vozoff 1972). For one dimensional AMT work, it is therefore necessary to choose two structural directions, one parallel to, and the other perpendicular to the strike (Cagniard 1953). When AMT soundings are carried out along profiles that are parallel or perpendicular to faults or intrusions, the location of these structures is made easier (Swift 1967, Vozoff 1972). One way to identify the structural directions when using scalar apparatus is to use the rotation method (Manguelle-Dicoum 1988).

The AMT data used for this study were collected using a scalar apparatus, the ECA 540 Resistivitymeter, with a frequency range of 4.1 – 2300 Hz. It measures the intensities of the electric and magnetic fields and calculates the apparent resistivities. The structural directions here were determined using the rotation method to be N30^{o}E, henceforth referred to as the longitudinal direction. This direction coincides with the overall direction of the line of volcanic centres that make up the CVL. The perpendicular direction, N120^{o}E is here referred to as the transverse direction.

Since the electric field E, the current I, and the resistivity ρ, are related through I = E/ρ; the vertical and horizontal discontinuities can more easily be seen by studying the behaviour of the electric field at a given station and along a given profile respectively. By observing the propagation of the electric field, it is easier to identify a conducting layer lying between two resistive ones. Hence, diagrams showing the variation of the electric field with frequency at each station have been used to provide a qualitative interpretation to the observed electric field along each profile in terms of the possible number of layers.

3. Results

AMT soundings were done at nine stations along two profiles; five stations along profile A: Bachuo-Akagbe (A1), Mbinjong (A2), Mbio (A3), Bakebe (A4) and Tinto (A5); and four stations along profile B: Nfeitok (B1), Etoko (B2), Etoko Mile 24 (B3) and Etoko Mile 25 (B4). The station coordinates are given in table 1 and these stations are shown on figure 2. Two telluric lines were used: one in a N30°E direction, parallel to the structural direction and the other in a N120 °E direction, perpendicular to the structural direction.

Table **1**. AMT stations showing their distance from reference point (origin) for each profile.

Profile A

Station Name	Station Code	Station Longitude	Station Latitude	Station Altitude (m)	Distance from A1 (km)
Bachuo-Akagbe	A1	09°27.342’	05°40.692’	195	0
Mbinjong	A2	09°28.551’	05°39.055’	167	3.8
Mbio	A3	09°30.664’	05°36.687’	235	10.2
Bakebe	A4	09°33.079’	05°34.972’	195	15.6
Tinto	A5	09°34.148’	05°33.663’	184	19.4

Profile B

Station Name	Station Code	Station Longitude	Station Latitude	Station Altitude (m)	Distance from B1 (km)
Nfeitok	B1	09°29.387’	05°43.543’	150	0
Etoko	B2	09°33.431’	05°43.485’	110	7.2
Etoko mile 24	B3	09°34.403’	05°41.916’	260	10.0
Etoko mile 25	B4	09°34.778’	05°42.178’	110	10.6

3.1 *Propagation of the electric field*

The analysis of the electric field is based on a diagram showing its variation with frequency (or depth) along any given profile (figures 3 and 4). The values of the electric field plotted here are mean values of three to five readings, each of them being an average of 5 repeated readings. Each of the five readings per data point was retained on the condition that it lies within 10% of the average. In so doing outliers were systematically eliminated.. The lateral propagation of the electric field along the N30°E telluric line shows a significant distortion of its signal between stations A1 and A2 and between A4 and A5 (figure 3a). Meanwhile the electric field seems to propagate in a similar way at stations A2, A3 and A4 since their plots present similar features. It is observed from the intensity of the electric field that current tends to flow into more conducting layers located between resistive ones. The intensity of the electric field is greatest for the low frequencies except at A5. Three parts stand out clear: a part with low frequencies, a middle part and a third part with high frequencies. This suggests that they could be about two interfaces giving 3 layers beneath each of these stations. Therefore, it is possible to propose the number of layers under each station by simply observing the variation of the electric field intensity with frequency for each station and across a profile. Similar observations can be made on the other telluric line (figure 3b) though the intensities are higher and distortion is now seen from A3 to A5. Therefore, two lateral transition areas are possible along profile A, the first between A1 and A2, and the second from A3 to A5.

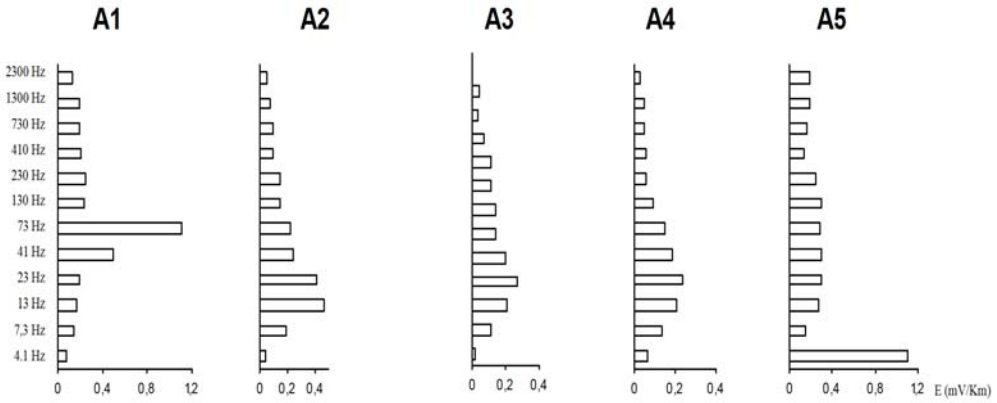

Figure **3a**. Propagation of E along profile A telluric line N30°.

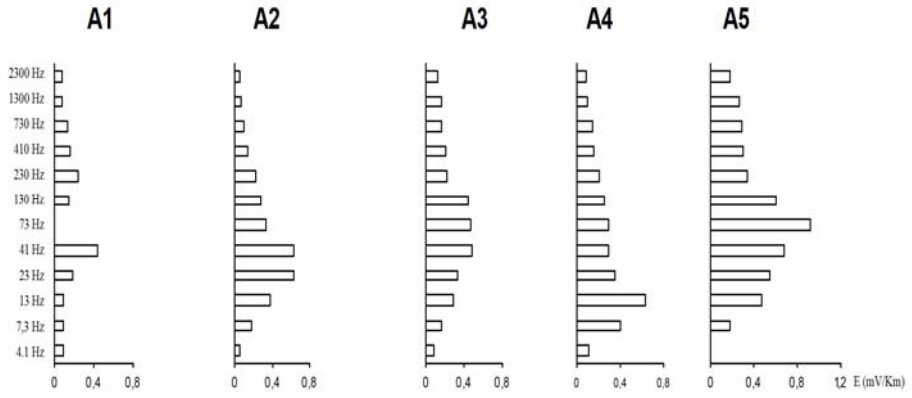

Figure **3b**. Propagation of E along profile A telluric line N120°.

Along profile B, stations B1 and B2 are so far apart (7.2km) that B1 can best be treated in isolation. However, a significant variation in the electric field is observed between B2 and B4 in both telluric directions (figure 4). The main reason for this distortion is that the study area is a transition zone between sedimentary and metamorphic rocks. The maximum intensities of the electric field are found at station B3 on both telluric lines. In general, the electric field in both telluric directions can also be separated into three groups suggesting the presence of 3 layers every where along this profile except along telluric line N120^{o}E (figure 4a) where up to five layers can be perceived.

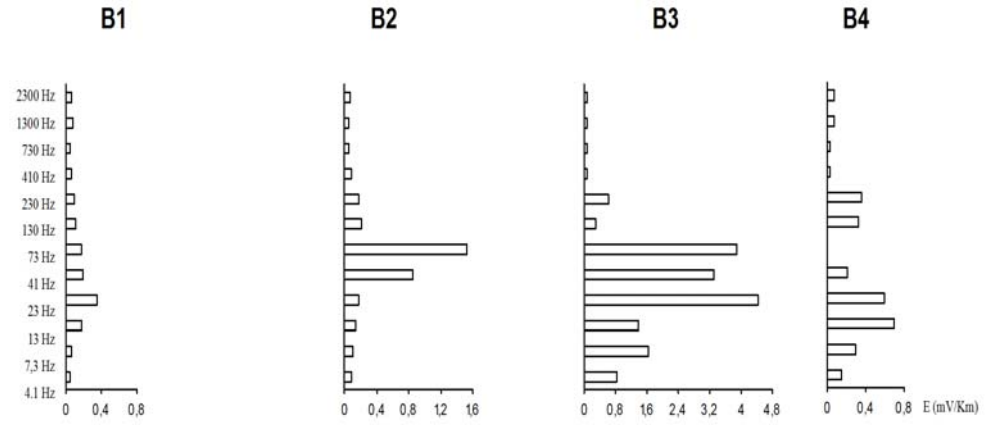

Figure **4a**. Propagation of E along profile B telluric line N120°.

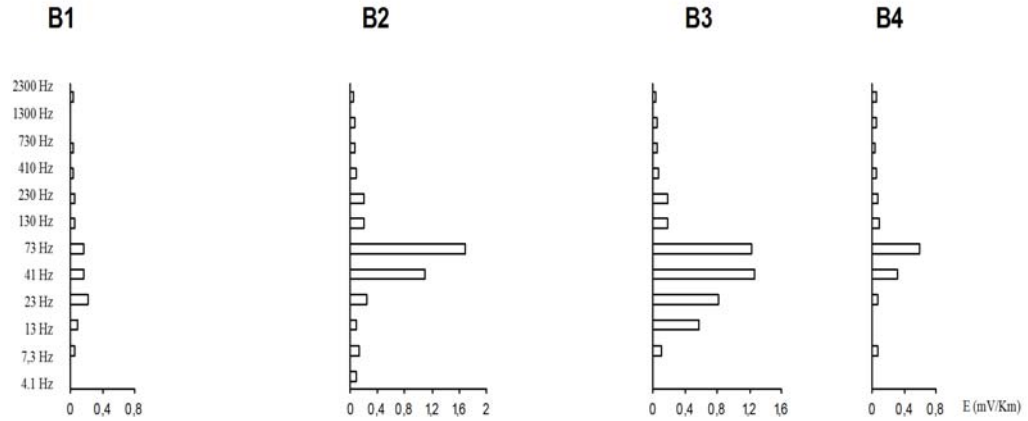

Figure **4b**. Propagation of E along profile B telluric line N30°.

3.2 *Frequency profiling*

In frequency profiling the apparent resistivity is plotted against the distance for each frequency along a profile. The plots have been separated into two frequency groups for clarity (4.1 – 73Hz and 130-2300 Hz). The apparent resistivity are each an average of five readings. Practically, the readings were retained only if the separate readings per frequency did not differ by a factor more than 2. This condition led to a data set (for each frequency) exhibiting very little scatter. Figures 5 and 6 show the frequency profiling along both N120°E and N30°E telluric lines for the two profiles. An increase of resistivity is observed between stations A1 and A2 for most frequencies except 4.1 Hz, along the N120°E telluric line. Between A2 and A3, resistivity lines are parallel but they gradually increase for frequencies 4.1 to 73 Hz. Minimum resistivities are observed at station A4 for the two telluric lines (figures 5 and 6). A significant decrease in resistivity is observed between A1 and A2 along the N30^{o}E telluric line (figure 6b), suggesting the presence of an anomaly around station A1. There is also a change in the earth structure between station A3 and A5 reflected in the low resistivities observed at A4. The subsurface seems to be generally homogeneous between A2 and A3 (resistivity lines are almost horizontal).

Figures 7 and 8 show the frequency profiling for profile B. Generally, the resistivity varies in a similar way along the two directions. A gradual increase of resistivity is observed between B1and B2 (figure 7) while the minimum resistivity is found at station B3 pointing to a possible fault between B2 and B4.

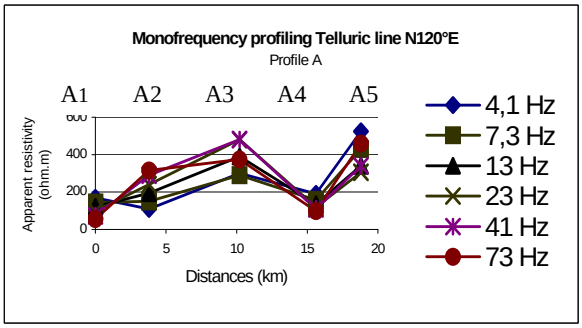

(a)

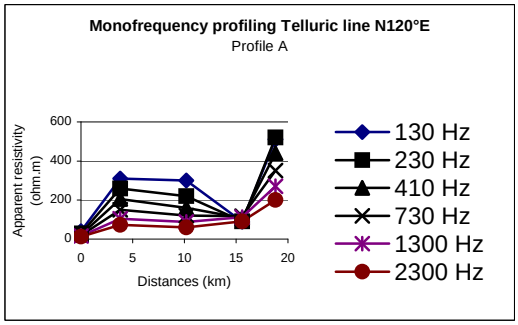

(b)

Figure **5.** Frequency profiling for profile A in the transverse direction.

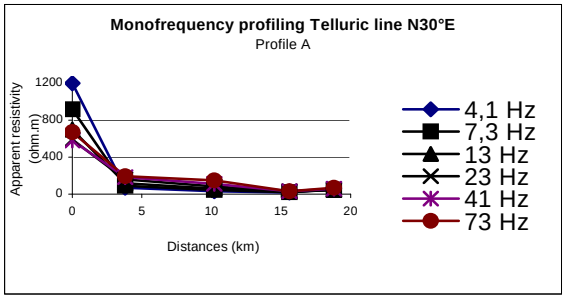

(a)

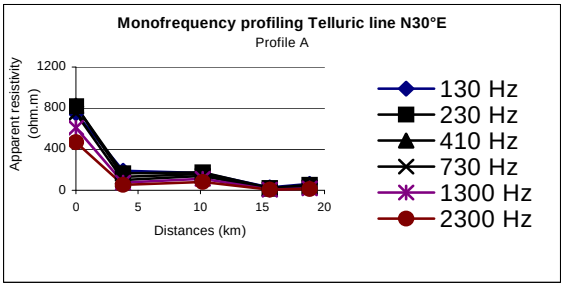

(b)

Figure **6.** Frequency profiling for profile A in the longitudinal direction.

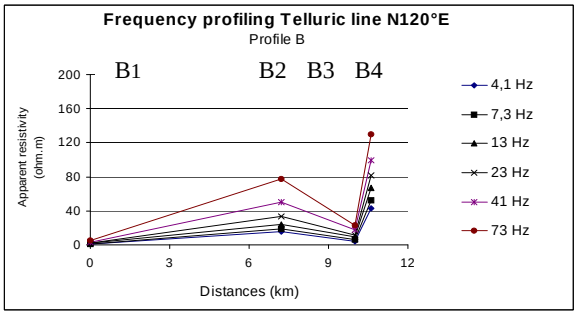

(a)

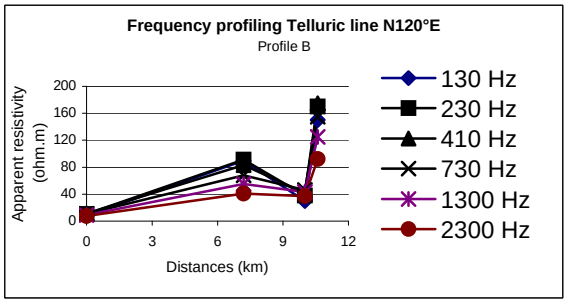

(b)

Figure **7**. Frequency profiling for profile B in the transverse direction.

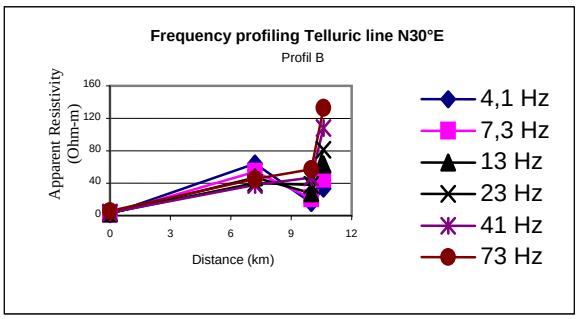

(a)

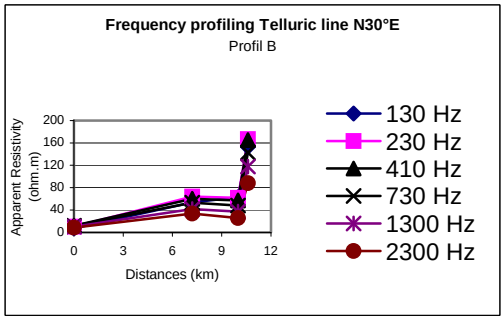

(b)

Figure **8.** Frequency profiling for profile B in the longitudinal direction.

3.3 *Pseudosections*

Pseudosections are curves of isoresistivity plotted along a profile showing both lateral and vertical variations of resistivities. Horizontal discontinuities are more easily identified by transverse apparent resistivities than by the longitudinal ones (Swift 1971, Manguelle-Dicoum et al 1992).

On the N120°E telluric line (figure 9a), both lateral and horizontal variations are observed from A1 to A2. The contour lines tend to be rather parallel and horizontal between A2 and A3, and then lateral variation in the resistivity is observed between A4 and A5 with a high gradient (figure 9a). On the N30°E telluric line (figure 9b), a lateral variation with high gradient (contour lines are almost vertical) is observed between A1 and A2. The contour lines are almost circular between A2 and A4 and there is a gradual lateral variation of resistivity from A3 to A5. The phenomenon observed between A1 and A2 is also seen from the electric field plots in figure 3.

In both directions of the telluric line, the resistivity varies laterally between stations B2 and B4 (figure 10a and 10b). There is a steep gradient between B2 and B4. The contour lines between B2 and B4 suggest a possible vertical movement as indicated by the arrow.

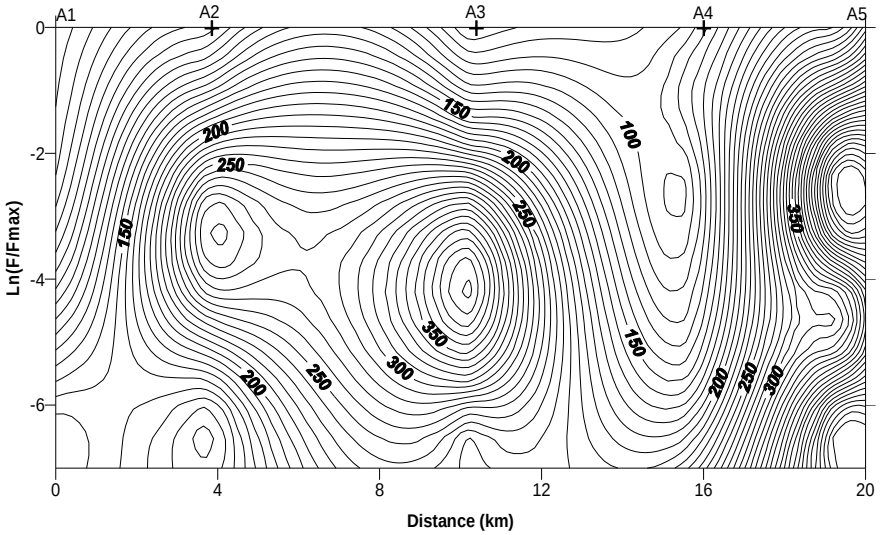

(a) Transverse

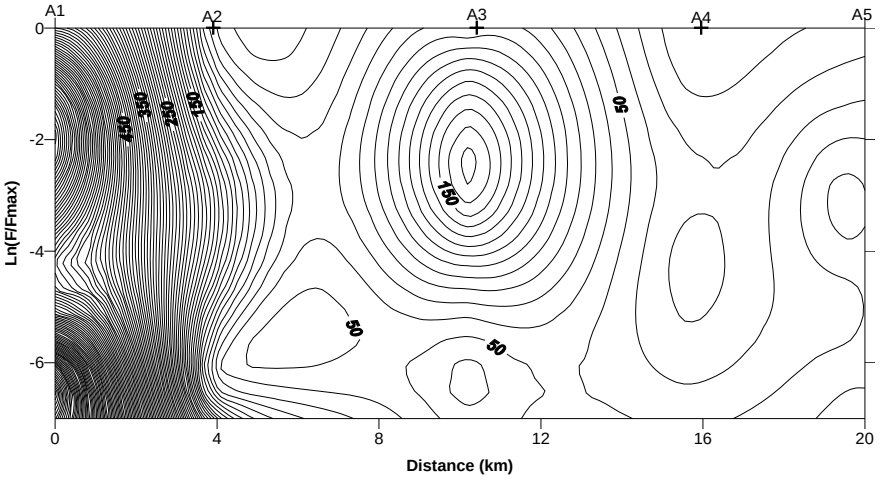

(b) Longitudinal

Figure **9.** Pseudosection for profile A.

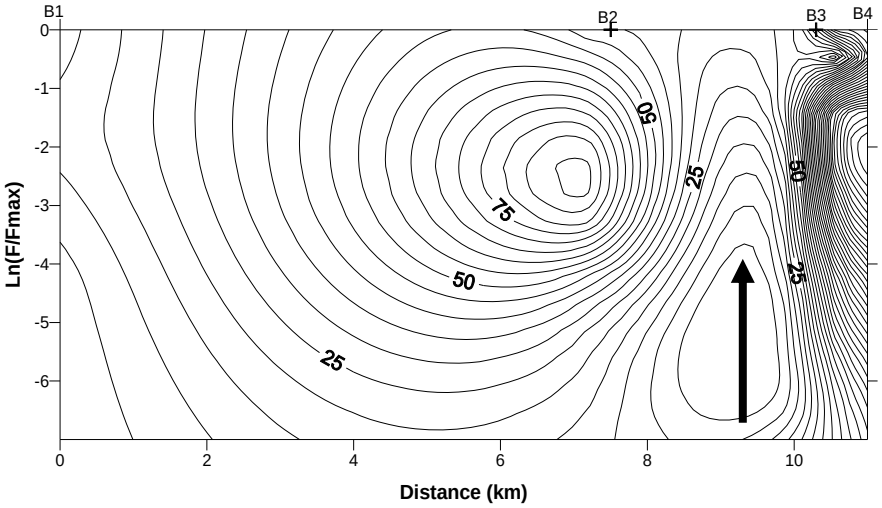

(a) Transverse

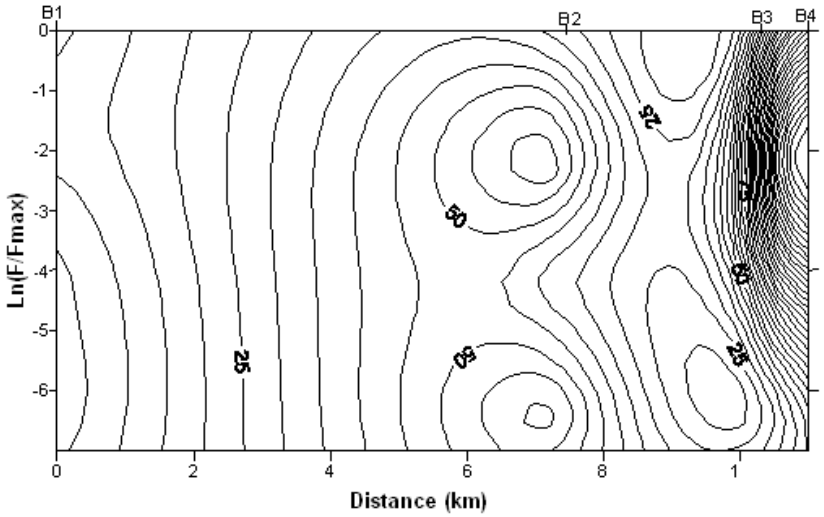

(b) Longitudinal

Figure **10.** Pseudosection for profile B (arrow shows possible vertical motion of block).

3.4 *Sounding curves*

For each station and each telluric line, interpretation of sounding curves in tabular models (Cagniard 1953) shows the distribution of subsurface layers characterized by their resistivities and thicknesses. On the N120°E telluric line of profile A, three-layer models were obtained at the station A1 and four-layer models at the other stations. In the N30^{o}E telluric direction four-layer models were obtained at all the stations. At station A1, for example, sounding curves along the two directions cannot be superposed, as illustrated in figure 11. This is further proof of heterogeneity.

Sounding curves of profile B along the N30°E telluric line, are interpreted as 3 layer models at station B1 and 4 layer models at the other stations, while curves along the N120°E telluric line are interpreted as 5 layer models at B2 and 4 layers model at the other stations.

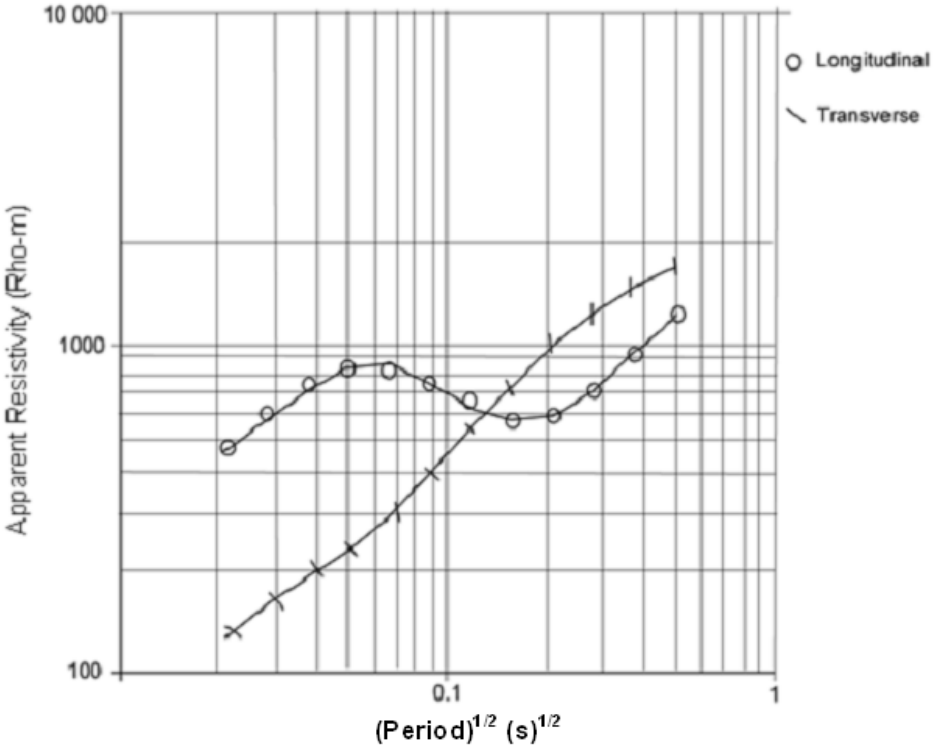

Figure **11**. Transverse and longitudinal sounding curves of station A1. Symbols represent the experimental points.

In general, the sounding curves for stations located inside the basin show that the low frequency part decreases with decreasing frequency. Meanwhile, at off-basin stations like A1 (figure 11), the resistivity increases with decreasing frequency corresponding to a half-space having higher apparent resistivity than the overburden.

3.5 *Geoelectric sections*

This is a representation of the model obtained from the interpretation of sounding curves at each station along a profile (figures 12 and 13). These figures show the layer resistivities and the geological formations as inferred from the local geology. Since the longitudinal geoelectric section better expresses the vertical variation of resistivities than the transverse geoelectric section and because resistivity variations are difficult to correlate close to faults, only the longitudinal geoelectric sections are presented here. The non uniqueness of the inversion of magnetotelluric data is a well known problem (Parker and Whaler, 1981; Simpson and Bahr, 2005; Israil et al, 2008). Optimum fitting of the data to the model was sort by adjusting the starting model in order to have a satisfactory fit. In most cases, a good fit (to within 90% Chi-squared test) was obtained. The longitudinal geoelectric section for profile A is given in figure 12. It shows near surface layers of relatively high resistivity (200 to more than 1000 Ohm-m). At stations A2 and A3 a resistive layer is found squeezed between conducting ones. The layers at stations A4 and A5 are alternately conducting and resistive, with resistivities up to 170 Ohm-m for station A4 and 240 Ohm-m for station A5. The maximum depth explored along this profile is about 1.4 km at station A1. From the relatively high resistivity of the last layer at station A5 (240 Ohm-m), it is possible that the basement has been sampled here.

The longitudinal geoelectric section for profile B (figure 13) presents three very highly conducting layers at station B1. Station B2 has resistive second and fourth layers while the others are

conducting. Stations B3 and B4 both have a resistive second layer, while others are conducting. There is a general decrease of resistivity with depth at all the stations of this profile. Such low resistivity values indicate that the basement was not sampled along this profile.

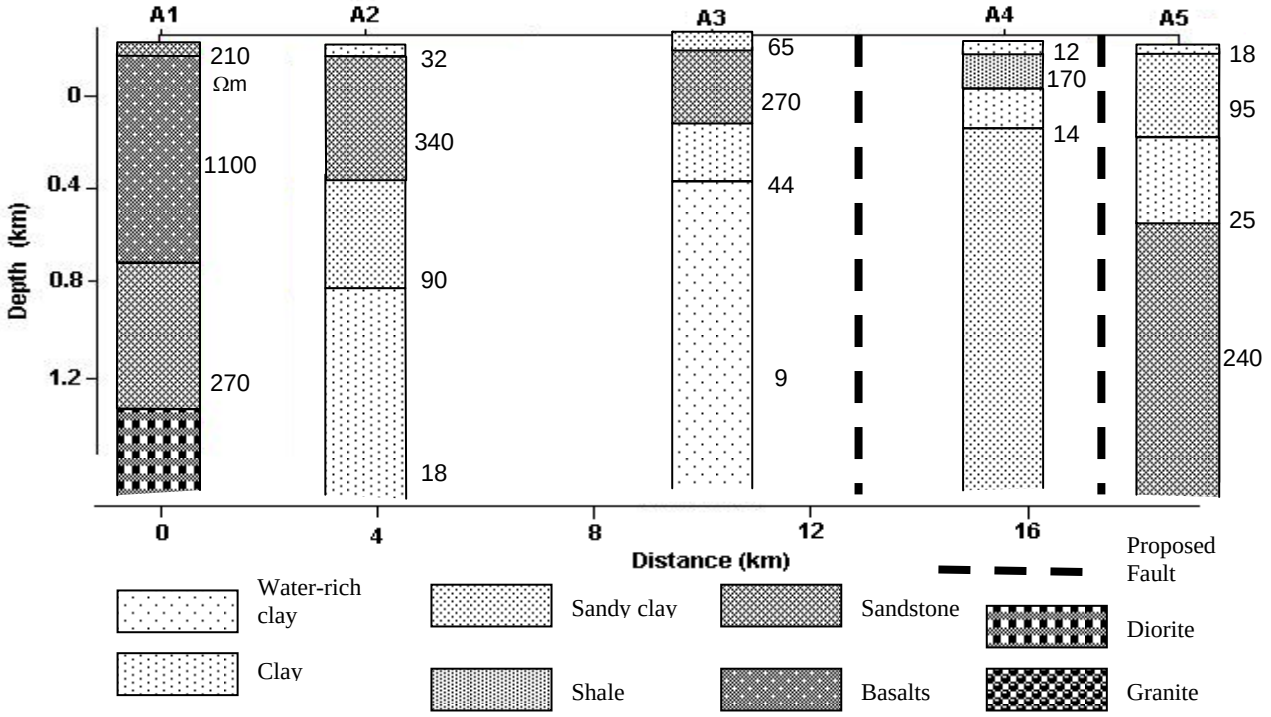

Figure **12.** Longitudinal geoelectric section of profile A. Numbers represent resistivities in Ohm-m.

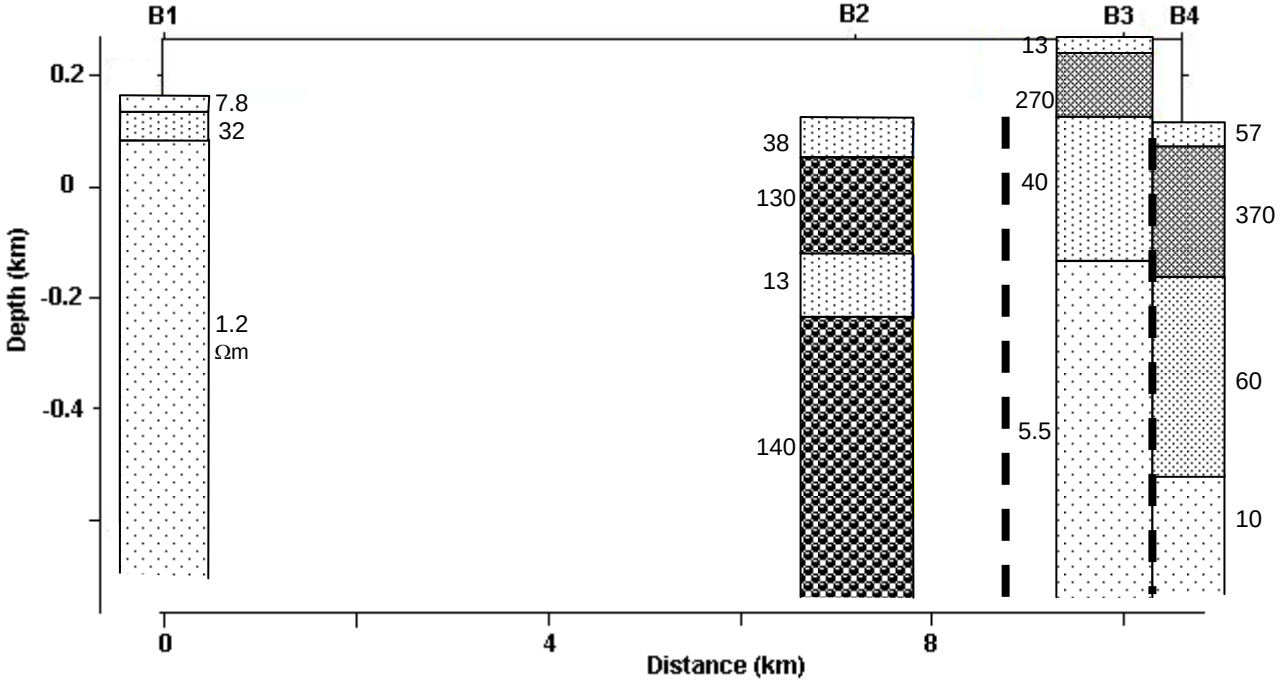

Figure **13.** Longitudinal geoelectric section for profile B.
(See figure 12 for legend).

Although it is obvious that the same experimental data set gives a more precise determination of the resistivity structure of a given study area when simpler (rather than complicated) models are used it remains true that the real earth is not that simple. The resolving power of the data was determined for each sounding curve using as resolution criterion, the quantity (Panza, 1981):

$$\left[\frac{1}{N}\sum_{j=1}^{N}\left(\partial\rho_{aj}/\partial P_i\right)^2\left(\sigma_j\right)^{-2}\right]^{-1/2}$$

where ρ_{aj} is the jth apparent resistivity, N is the total number of readings per site (in this case, 12), σ_j is the error in the resistivity readings (assumed to be the same for all readings) and P_i is the ith parameter.

Table 2 shows typical resolution values for 4-layer and 3-layer models at two different sites. As can be seen from this table, most of the parameters are quite well resolved.

Table **2**: Resolution of layer thickness and resistivity at two stations **(A3)** and **(B1)**.

A3					**B1**				
Layer	**Resistivity(Rho-m)**		**Thickness**		**Layer**	**Resistivity(Rho-m)**		**Thickness**	
No.	**Value**	**Resolution**	**Value**	**Resolution**	**No.**	**Value**	**Resolution**	**Value**	**Resolution**
1	65	***0.3***	42	***0.2***	**1**	7.8	***0.5***	24	***1.7***
2	270	***1.1***	340	***1.4***	**2**	32	***2.3***	48	***3.4***
3	44	***0.2***	250	***1.1***	**3**	1.2	***0.1***		
4	9	***0.1***							

4. Discussion

The resistivity models obtained from the electric field, sounding curves, frequency, pseudosection and geoelectric section plots suggest that the anomaly around station A1 is an intrusion not withstanding the fact that the profile did not cross it. The high resistivities under A1 are therefore interpreted to represent igneous rocks. This therefore redefines the extent of the igneous intrusion mapped out on the geological map (figure 2). The complexity of the structure under stations A3, A4, A5 and B2, B3 and B4 is evident through the fact that all these stations have a highly resistive near surface layer of resistivity varying between 95 and 340 Ohm-m. The basement is sampled only at A5. The lateral variation of transverse resistivities between A3, A4 and A5, as seen in figure 5, suggests that faulting has occurred between stations A3 and A5 which has been represented by broken lines in figure 12. The regional tectonic forces responsible for the emplacement of the intrusion around A1, coupled with the activity along the suggested fault(s) could have resulted in the presence of such material of high resistivity within sediments since resistivities similar to those of sediments are found below these resistive layers. Therefore, the presence of these layers of high resistivities close to the surface could be the effect of the intrusions having been dislocated by the faulting and tectonic activities. These tectonic forces must be the same forces (probably extension) that were responsible for the formation of the Benue trough in Nigeria located to the west of the Mamfe basin. It is usually difficult to give adequate interpretation to 1-D data in complex geological environments, for example near faults (Manguelle-Dicoum et al 1993) as is the case in this study. The presence of these faults is also

depicted on the electric field plots (figures 3 and 4). The results generally reveal the high heterogeneity of rocks at the eastern border of the basin which can be located between A4 and A5 along profile A.

The resistivities observed along profile B are generally lower than those along profile A. This can easily be seen on the frequency profiling diagrams (figures 5-8). The low resistivity values at B1 indicate that it is located in the basin, way off the basin edge, and that its proximity to the flood plain of river Manyu may be influencing these resistivity values. The presence of only low resistivities long profile B especially at station B4 suggests that the basement was not sampled along most of this profile. However, the relatively high resistivity of the fourth layer at station B2 suggests the presence of some igneous material, probably granite, intruding under this station as earlier suggested by Dumort (1968). This is evident on the pseudosection (figure 10) where the arrow shows the possible direction of vertical motion of the material. It is therefore possible that faulting has occurred between stations B2 and B5 as represented in figure 13 by the broken lines. The reactivation of these faults coupled with other regional tectonic movements may be the origin of the high resistivities observed at shallow depth. The distortion observed on the electric field diagrams further confirms this. The presence of low resistivities of about 10 Ohm-m at B4 could be due to the presence of the water table at a depth of less than 500 m. The limit of the basin along profile B is marked by the fault which could be located between B3 and B4. The resolution of the data was even found to be poorer (in absolute values) for a simpler model (see 3-layer model in Table 2). Obviously, the availability of independent a priori information coming from geology, geophysics and other works, should greatly contribute to the reduction of the uniqueness problem. In our case, the constrains to the models is mainly from geology which is not very detailed.

5. Conclusion

The geophysical investigation of the eastern margin of the Mamfe basin using audio-magnetotelluric method has revealed a basement-sediment transition zone along the two profiles studied, demarcated by faults possibly located between stations A3 and A5 on profile A and stations B2 and B4 on profile B. Stations A4 on profile A and B3 on the profile B are located within these fault systems. The eastern limit of an intrusion identified from geology close to station A1 along profile A in the eastern part of the Mamfe basin has been redefined. Another basement intrusion has also been identified at station B2 along profile B. It is however very clear that the limits of the basin as studied here are overshadowed by the transition zone between basin sediments and metamorphic rocks at the edge of the basin. The complexity noticed here is probably the result of past faulting which led to the emplacement of the basin, rather than recent tectonic activity. Although local seismicity in the basin area has not been investigated, the region, in general, has no history of significant seismicity. However, the audio-magnetotelluric data analysed in this study, has given models that agree reasonably well with the local geology and so provide the first resistivity earth models in this part of the basin.

Acknowledgments

This study was financed by the National Hydrocarbon Cooperation (SNH) Cameroon. One of the authors (C T Tabod) is grateful to the Abdus Salam International Centre for Theoretical Physics (ICTP), Trieste, Italy, which through its Associate Federation Scheme with support from the Swedish International Development Agency (SIDA), sponsored his stay at the ICTP during which part of this work was done.

References

Cagniard L 1953 Principe de la méthode magnétotellurique, nouvelle méthode de prospection géophysique *Ann. Geophys.* **9** 95-124

Collignon F 1968 Gravimétrie de reconnaissance de la République Fédérale du Cameroun *ORSTOM Paris France* 35p

Dumort J C 1968 Notice explicative sur la feuille de Douala-Ouest. Carte géologique de reconnaissance *Direction des mines et de la géologie du Cameroun* 69 pp

Fairhead J D and Green C M 1989 Controls on rifting in Africa and the regional tectonic model for the Nigeria and East Niger rifts basins *Journal of African earth sciences* **8(2-4)** 231-249

Fairhead J D and Okereke C S 1987 A regional gravity study of the West African rift system in Nigeria and Cameroon and its tectonic interpretation *Tectonophysics* **213** 459-481

Fairhead J D and Okereke C S 1988 Depth to major contrast beneath the West African rift system in Nigeria and Cameroon based on the spectral analysis of gravity data *Jour. of African Earth Science* **7(5-6)** 769-777

Fairhead J D Okereke C S and Nnange J M 1991 Crustal structure of the Mamfé basin, West Africa, based on gravity data *Tectonophysics* **186** 351-358

Fuji-ta K, Ogawa Y, Yamaguchi S and Yaskawa K 1997 Magnetotelluric imaging of the SW Japan forearc-a lost paleoland revealed? *Phys. Earth and Planetary Interiors* **102** 231-238

Israil M, Tyagi D K, Gupta P K and Niwas S. 2008 Magnetotelluric investigations for imaging electrical structure of Garhwal Himalayan corridor, Uttarakhand, India *J. Earth Syst. Sci.* **117** 189-200

Kande H L 2000 Etude Audiomagnétotellurique de la transition sédimentaire-métamorphique de la bordure orientale du bassin de Mamfé, Cameroun *Mémoire de Maîtrise* Université de Yaoundé I 60p

Lilley F E M, Wang L J, Chamalaun F H and Ferguson I J 2001 The Carpentaria electrical conductivity anomaly, Queensland, as a major structure in the Australian plate *GSAA monograph* **201** 1-16

Manguelle-Dicoum E 1988 Etude géophysique des structures superficielles et profondes de la région de Mbalmayo (Cameroun) *Thèse de Doctorat d'Etat Université de Yaoundé*

Manguelle-Dicoum E Bokosah A S and Kwende Mbanwi T E 1992 Geophysical evidence for a major Precambrian schist-granite boundary in Southern Cameroon *Tectonophysics* **205** 437-446

Manguelle-Dicoum E Nouayou R Bokosah A S and Kwende Mbanwi T E 1993 Audiomagnetotellurics (AMT) soundings on the basement-sedimentary transition zone around the Eastern margin of the Douala Basin in Cameroon *Journal of African Earth Sciences* **17(4)** pp. 487-496

Monteiro Santos F A, Trota A, Soares A, Luzio R, Lourenco N, Matos L, Almeida E, Gaspar J L and Miranda J M 2006 An audio-magnetotelluric investigation in Terceira island (Azores) *J. Applied Geophys.* **59** 314-323

Ngando A M Tabod CT Manguelle-Dicoum E Nouayou R Jean Marcel Zakariaou A 2004 Structure géologique le long de deux profils audio-magnétotelluriques dans le bassin de Mamfé, Cameroun. *Journal of Cameroon Academy of Sciences,* **4(2)** 149-164

Ndougsa Mbarga T 2004 Etude géophysique par méthode gravimétrique des structures profondes et superficielles de la région de Mamfe. Investigation régionale du bassin sédimentaire et des zones non-sédimentaires avoisinantes: évolution du socle granito-gneissique et géométrie du bassin. Evaluation de la capacité réservoir du bassin *Thèse de Doctorat/Ph. D. de Physique, Spécialité Géophysique Interne. Université de Yaoundé I*

Ndougsa Mbarga T Manguelle-Dicoum E Bisso D Njingti N 2004 Geophysical evaluation based on the Gravity Data of the Mamfe basin, South West Cameroon (Central Africa) *SEGMITE International* **1** 4-10

Nouayou R 2005 Contribution à l'étude géophysique du bassin sédimentaire de Mamfe par prospections audio et hélio magnétotelluriques *Thèse de Doctorat d'Etat ès sciences, spécialité Géophysique Interne, Université de Yaoundé I* 184p

Nurhasan, Ogawa Y, Ujihara N, Tank S B, Honkura Y, Onizawa S, Mori T and Makino M 2006 Two electrical conductors beneath Kusatsu-Shirane volcano, Japan, imaged by audiomagnetotellurics, and their implications for the hydrothermal system *Earth Planets Space* **58** 1053-59

Ogawa Y, Takakura S and Honkura Y 2002 Resistivity across Itoigawa-Shizuoka tectonic line and its implications for concentrated deformation *Earth Planets Space* **54** 1115-20

Panza G 1981 The resolving power of seismic surface waves with respect to crust and upper mantle structural models. *In : The solution of the inverse problem in Geophysical Interpretation, R. Cassinis (ed.), Plenum Press.* 39-77

Parker R. L and Whaler K A 1981. Numerical methods for establishing solutions to the Inverse problem of Electromagnetic Induction. *J. Geophys. Res.* Vol. **86.** No. B10 9574-9584

Paterson, Grant and Watson Ltd 1976 Etudes aéromagnétiques sur certaines régions de la République Unie du Cameroun *Rapport d'interprétation Agence Canadienne de Développement International Toronto*

Simpson F and Barh K 2005, Practical magnetotellurics *Cambridge University Press*

Swift C M R 1967 Magnetotelluric investigation of an electrical conductivity anomaly in South Western United States. *PhD Thesis Department of Geology and Geophysics* MIT.

Swift C M R 1971 Theoretical magnetotelluric and turam response from two-dimensional inhomogeneities *Geophysics* **36** 38

Vozoff K 1972 The magnetotelluric method in the exploration of sedimentary basins *Geophysics* **37**: 98-141